

# The Development of a Novel High Throughput Computational Tool for Studying Individual and Collective Cellular Migration

Douglas A. Chapnick, Jeremy Jacobsen, Xuedong Liu\*

Department of Chemistry and Biochemistry, University of Colorado, Boulder, Colorado, United States of America

## Abstract

Understanding how cells migrate individually and collectively during development and cancer metastasis can be significantly aided by a computation tool to accurately measure not only cellular migration speed, but also migration direction and changes in migration direction in a temporal and spatial manner. We have developed such a tool for cell migration researchers, named Pathfinder, which is capable of simultaneously measuring the migration speed, migration direction, and changes in migration directions of thousands of cells both instantaneously and over long periods of time from fluorescence microscopy data. Additionally, we demonstrate how the Pathfinder software can be used to quantify collective cell migration. The novel capability of the Pathfinder software to measure the changes in migration direction of large populations of cells in a spatiotemporal manner will aid cellular migration research by providing a robust method for determining the mechanisms of cellular guidance during individual and collective cell migration.

**Citation:** Chapnick DA, Jacobsen J, Liu X (2013) The Development of a Novel High Throughput Computational Tool for Studying Individual and Collective Cellular Migration. PLoS ONE 8(12): e82444. doi:10.1371/journal.pone.0082444

**Editor:** Joshua Z. Rappoport, University of Birmingham, United Kingdom

**Received:** July 26, 2013; **Accepted:** October 23, 2013; **Published:** December 27, 2013

**Copyright:** © 2013 Chapnick et al. This is an open-access article distributed under the terms of the Creative Commons Attribution License, which permits unrestricted use, distribution, and reproduction in any medium, provided the original author and source are credited.

**Funding:** D.A.C. was supported by a predoctoral training grant from NIGMS (T32GM08759). This work was supported by grants by US Army grant no. W81XWH-10-1-0989 and the National Institutes of Health (R01GM083172 and R01CA107098) to X.L. The ImageXpress MicroXL was supported by a NCRP grant S10 RR026680 from NIH.

**Competing Interests:** The authors have declared that no competing interests exist.

\* E-mail: liux@colorado.edu

## Introduction

Cellular migration has been shown to be an important process in cancer progression, development, tissue repair, and immune response [1–10]. As a result, a plethora of research has been performed to identify the molecular mechanisms behind how individual cells achieve migration, as well as how neighboring cells migrate cooperatively in collective migration (reviewed in [11–13] and [14], respectively). Collective migration is defined as the ability of physically interacting cells to adopt a common migration direction [14,15]. Like individual cell migration, the collective migration of cells has been shown to be an important process in cancer progression, development and wound repair [16–23]. Such collective behavior results from each cell responding to the environmental stimuli of neighboring cells, in addition to non-cell environmental stimuli [4,5,14,15,17,19,20,24–32]. Although a relatively large amount of research has been conducted to determine mechanisms behind individual cell migration, far less is known about exactly how cells migrate collectively. Furthermore, there is no standard method in the literature to quantify the ‘collectiveness’ behavior during collective migration [33–35].

Previous research into individual cell migration has revealed important fundamental mechanisms by which cells migrate. For instance, when an individual cell migrates on a two-dimensional (2D) surface, it projects a front end extension that can either be broad (termed a lamellipodia) or with multiple spike-like extensions (termed filipodia), which are the result of coordinated polymerization, depolymerization, and branching of the actin cytoskeleton [12,24,36–46]. Such coordination of actin dynamics

is controlled by local recruitment of cell polarity maintain proteins, such as CDC42/Rac and Rho, which either directly or indirectly regulate actin structure, polymerization, and attachment to the extracellular matrix [37,38,47–51]. The attachment of the actin cytoskeleton is largely mediated by protein complexes, termed focal adhesions, which anchor the actin cytoskeleton to trans membrane integrin receptors and the extracellular matrix [52]. The assembly of focal adhesions allows for the cell to successfully attach a front end extension to the extracellular matrix and the disassembly of focal adhesions allows a cell to detach the rear during rear end retraction [53–55]. Focal adhesion turnover and the resulting changes to the actin cytoskeleton are regulated by several kinase activities, including focal adhesion kinase (FAK), Src kinase and Rho GTPase [12,56–60]. The temporal and spatial regulation of both the actinomyosin skeleton and focal adhesions are regulated by a complex combination of growth factor signaling and extracellular matrix protein activities, which influence the speed of actin and focal adhesion dynamics, ultimately influencing how fast a cell can migrate [61,62].

Our current understanding of the biochemical mechanisms underlying cellular migration have been primarily the result of *in vitro* studies conducted in 2D cell culture model systems [2,11–13,24,31,32,38,40–43,54,56,57,60,62–70]. However, several critical biochemical activities governing cell migration have proven to play similar roles in three dimensional (3D) model systems and *in vivo*. For instance, in 2D, 3D and *in vivo* experiments, CDC42/Rac activity determine cellular polarity [71,72]. Similarly, FAK kinase mediates cellular migration both in 2D and 3D assays [73–75]. As

a result, investigations performed in 2D assays have shed light on biochemical mechanisms that have proven to have physiological relevance. However, recent research has also revealed that there is significant difference in cell migration machinery between cells in 2D versus 3D [75–77]. Although the conclusions made in 2D migration studies will always require confirmation of physiological relevance in *in vivo* studies, they remain a valuable tool for initial investigations into the molecular mechanisms behind cellular migration compared to 3D and *in vivo* studies because they allow for tight control of experimental conditions and more accurate observation of cellular migration behavior at single cell resolution without the use of relatively complex microscopes, such as two-photon and confocal microscopes. Many of the concerns about discrepancies in biochemical mechanisms behind 2D and 3D motility may prove to be overcome by imaging individual cell motility in 2D on soft extracellular matrices, which have been shown to be more closely similar to *in vivo* tissues than plastic or glass cell culture plates [78].

The behavior of migrating cells can be characterized by migration speed, migration direction, and migration persistence (the ability of a cell to maintain its migration direction). In 2D studies, the measurement of cell migration behavior is conducted by either manual cell tracking [79–81] or automated cell tracking [31,32,61,82–85]. Such cell tracking experiments have not only shed light on how a cell achieves migration, but also have shown that cells can undergo chemotaxis towards a localized biochemical signals [20,86,87]. In these studies, a Dunn Chamber is used to present a chemokine gradient to cells, where cells migrate upstream of Epidermal Growth Factor (EGF) and Urokinase Plasminogen Activator (uPA) gradients [88]. Such studies into how cells achieve chemotaxis highlight the need for cell migration tracking programs to not only calculate the speed and persistence of cells, but also to report the direction and changes in direction during cellular migration.

Although several computational tools exist that allow for automated cell tracking of individual cells in time-lapse microscopy videos (**Fig. 1**), these tools focus almost entirely on either the speed or persistence (ability to maintain a migration direction) or a cell. We have developed an automated high throughput cell tracking software, named Pathfinder, which is capable of simultaneously measuring and reporting cellular migration speed, migration direction and changes in migration direction of thousands of fluorescently labeled cells for an unlimited number of microscopy videos. The Pathfinder software has two improved features that distinguish it from previous cell motility computational tools, as the Pathfinder output is able to report instantaneous cell migration direction and changes in cellular migration direction. Although the cellular migration field has elucidated many fundamental mechanisms behind cellular migration, there are several key questions that remain to be answered. Specifically, ‘how does a cell select a migration direction?’ and ‘what makes a cell change direction?’ Answering these questions will require the ability to study the migration direction and changes in migration direction at single cell and instantaneous resolution. Additionally, we explain how measurements of cellular migration direction can be used to quantify collective migration. In summary, the Pathfinder software aims to propel the cell migration field forward in both the mechanistic understanding of individual cell migration, as well as collective cell migration by allowing researchers to fully characterize cell migration behavior in an automated and high throughput manner.

## Methods

### Fluorescent Labeling of Cells, Cell Culture and Cellular Imaging

Stable transgenic HaCaT (Cell Lines Services, Germany) and MDA-MB-231 (ATCC, HTB-26) cell lines were fluorescently labeled via retroviral mediated gene transfer of mCherry-Histone H2B using the pRex-mCherry-H2B plasmid. For all experiments, cells were cultured in DMEM lacking phenolphthalein red and supplemented with 2 mM L-glutamine, 100 Units/mL penicillin and 100 µg/mL streptomycin. For low density assays, cells were plated at an average density of 300 cells/mm<sup>2</sup> for both HaCaT and MDA-MB-231 cells. For confluent monolayer experiments, HaCaT cells were plated at an average density of 1000 cells/mm<sup>2</sup>. For epithelial sheet assays, HaCaT cells were plated at an average density of 1200 cells/mm<sup>2</sup> for 3 hours at 37°C, after which half of partially adherent cells were manually removed using a 200 µl pipet tip. Transforming Growth Factor-Beta (TGFβ) stimulations were conducted with 100 pM ligand, while EGF stimulations were conducted with 100 nM ligand. An ImageXpress MicroXL high throughput wide-field fluorescence microscope (Molecular Devices) was used for imaging experiments at 37°C and 5% CO<sub>2</sub>. All microscopy videos were acquired with a frame rate of one frame every seven minutes, in the mCherry fluorescence channel at a magnification of 10×, where each pixel represents 1.314 µm at a pixel binning of 2×2. The accompanying MetaXpress software was used to compile video files from time-lapse images for each well of a 96 well plate.

### Programming, Input Parameters, and Output for the Pathfinder Software

The Pathfinder software (<https://universityofcolorado.box.com/s/qz6nos4470sjsaw8wg> and **Data S1**) was written in the Java programming language. User specification is required for cell radius (pixels), minimum track length, the interval of frames for desired calculations (frame n – frame n+a, where a represents the number of frames to skip for calculations), percentage of pixels in the video that represent cells, and the directory path for the folder containing .avi files (**Fig. S1**). The output for each video file is a single Excel spreadsheet (**Fig. S2 and Data S2**). The Pathfinder software requires only decompression of the attached .zip file and installation of JAVA runtime environment on either a 32-bit or 64-bit Windows Machine. Please note that use of pathfinder on a 64-bit machine allows for higher memory use in Java, which allows for analysis of greater numbers of cells in a single video.

### Calculation of Migration Parameters, Persistence Time and Nearest Neighbor Analyses

Cellular speed was calculated as the displacement of a cell (pixels) over 1 frame. Conversion to µm/hour is determined by the following equation:

$$\text{Conversion Factor} = \frac{(\text{Camera Pixel Size} \times \text{Binning Factor})}{(\text{Magnification Factor} \times \text{Frame Rate})}$$

The Angle of Trajectory was calculated from the following discontinuous equations:

$$\text{if } (dx > 0, dy > 0), \text{ then } \theta_{\text{trajectory}} = 360 - \text{ArcTAN} \left( \frac{dy}{dx} \right)$$

Software Name	Website URL	Position	Speed	Direction	Persistence
ImarisTrack	http://www.bitplane.com/go/products/imaristrack	✓	✓		
Volocity	http://www.perkinelmer.com/pages/020/cellularimaging/products/volocity.xhtml	✓	✓		
Cell Track	http://db.cse.ohio-state.edu/CellTrack/	✓	✓		
Cell Tracker	http://www2.warwick.ac.uk/fac/sci/systemsbiology/staff/bretschneider/celltracker	✓	✓		
Mtrack2	http://user.interface.org.nz/~gringer/hacking/mtrack3.html	✓	✓		
MetaMorph	http://www.bioimagingolutions.com/MolDev/metamorph_analysis.html	✓	✓		
Cell Motility Monitoring Project	http://genesis.ugent.be/cell_motility/distrib/distribution.html		✓		✓
Chemotaxis and Migration Tool	http://ibidi.com/xtproducts/en/Software-and-Image-Analysis/Manual-Image-Analysis/Chemotaxis-and-Migration-Tool		✓	✓	
Pathfinder	https://universityofcolorado.box.com/s/qzs6nos4470sifsaw8wg	✓	✓	✓	✓

**Figure 1. The Pathfinder cell motility program uniquely incorporates measurements of cellular position, speed, direction, and persistence.** Although several cellular motility programs are available to measure cellular motility in terms of position and speed, only the Pathfinder program additionally reports both cellular migration direction and cellular migration persistence.  
doi:10.1371/journal.pone.0082444.g001

$$\text{if}(dx > 0, dy < 0), \text{then } \theta_{\text{trajectory}} = -\text{ArcTAN}\left(\frac{dy}{dx}\right)$$

$$\text{if}(dx < 0, dy = 0), \text{then } \theta_{\text{trajectory}} = 180$$

$$\text{if}(dx < 0, dy > 0), \text{then } \theta_{\text{trajectory}} = 180 - \text{ArcTAN}\left(\frac{dy}{dx}\right)$$

$$\text{if}(dx = 0, dy < 0), \text{then } \theta_{\text{trajectory}} = 90$$

$$\text{if}(dx = 0, dy = > 0), \text{then } \theta_{\text{trajectory}} = 270$$

$$\text{if}(dx < 0, dy < 0), \text{then } \theta_{\text{trajectory}} = 180 - \text{ArcTAN}\left(\frac{dy}{dx}\right)$$

Angle of Deflection was calculated from the following discontinuous equations:

$$\text{if}(dx = 0, dy = 0), \text{then } \theta_{\text{trajectory}} = \text{No Angle}$$

$$\begin{aligned} \text{if}(\theta_{\text{Deflection}} \geq 180), \text{then } \theta_{\text{Deflection}} \\ = (\theta_{\text{Trajectory } t=n+1} - \theta_{\text{Trajectory } t=n}) - 360 \end{aligned}$$

$$\text{if}(dx > 0, dy = 0), \text{then } \theta_{\text{trajectory}} = 0$$

$$\begin{aligned} & \text{if}(\theta_{\text{Deflection}} \leq -180), \text{then } \theta_{\text{Deflection}} \\ & = (\theta_{\text{Trajectory } t=n+1} - \theta_{\text{Trajectory } t=n}) + 360 \end{aligned}$$

Persistence time calculations were performed using a modified in-house MatLab based program developed by Dr. Douglas Lauffenburger (MIT) (**Data S3**).

Nearest neighbor calculations were done in Excel using an inter-centroid distance matrix of (all cells) × (all cells) for each frame. Nearest neighbors were defined as cells whose centroids are within 100 μm of each other. Paired random migration index of the angle of trajectory (PRMI  $\Theta_{\text{Trajectory}}$ ) calculations were also done in Excel, where the standard deviation of the migration directions between pairs of neighboring cells were averaged over greater than 100 pairs of cells for each condition. This average of standard deviations is referred to as the PRMI  $\Theta_{\text{Trajectory}}$ .

## Results

### The overview and capabilities of the pathfinder software

The JAVA based Pathfinder software was developed to allow researchers to easily analyze large data sets of time-lapse fluorescence microscopy videos of motile cells. Since cellular tracking is already a well-established technique, our software implements a previously validated tracking algorithm ('Particle Tracker') developed by Sbalzarini *et al* to detect each fluorescently labeled nuclei in each frame (**Fig. 2A, left**), as well as to assemble such positional information into cellular tracks (**Fig. 2A, right**), as described in their publication [89]. Since cellular positions alone are of little use to researchers in the cell migration field, we developed an analysis algorithm to transform the previous 'Particle Tracker' output into an excel spreadsheet that displays calculations of the speed, the direction, and changes in direction of individual cells, as well as the average values for a population of cells (**Fig. 2B, S3, and S4**). Simultaneous reporting of these parameters makes the Pathfinder software unique compared to other available computational motility programs (**Fig. 1**). In addition, Pathfinder is capable of running batch parallel processing of unlimited .avi files, allowing for automated and high throughput data processing of fluorescent time-lapse microscopy videos, provided they are placed in a single folder that can be navigated to from within the Pathfinder GUI. The Pathfinder program requires either a 32 bit or a 64 bit windows operating system with JAVA Runtime Environment.

### Fluorescent Labeling of Cells Does not Significantly Alter Cell Motility

We compared the migration speeds of wild type MDA-MB-231 cells to MDA-MB-231 cells expressing a nuclear fluorescence marker in the presence and absence of EGF in order to determine if the introduction of nuclear marker significantly impacted ligand induced migration. Unlabeled wild type cells were manually segmented and analyzed using Pathfinder, while fluorescent images were automatically segmented and analyzed using Pathfinder. Introduction of a fluorescent nuclear marker into these cells did not significantly alter the EGF induced cellular migration speed (**Fig. S3**). However, we do not rule out that different methods of gene delivery and types of nuclear markers (for instance a fluorescent protein other than histone H2B) could lead to permanent changes in cell migration.

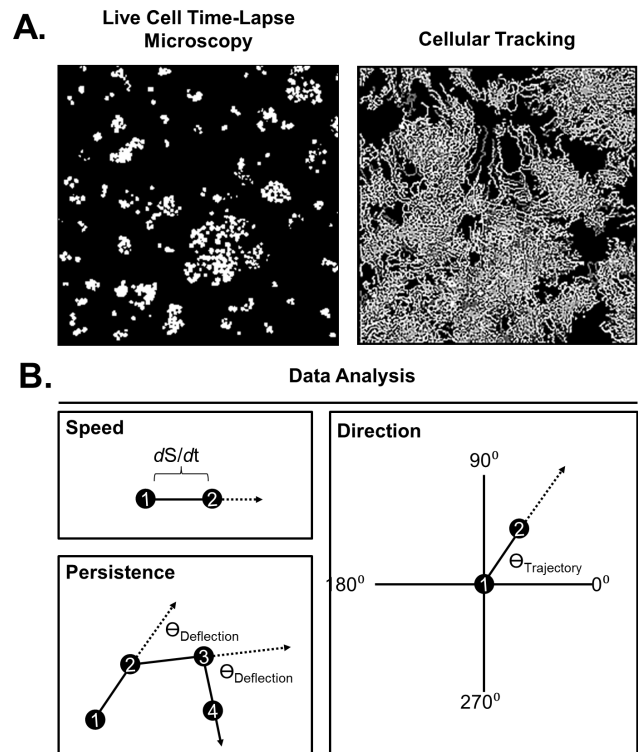


**Figure 2. Angular measurements of cellular migration can reveal cellular behavior.** **A)** The Pathfinder program converts time-lapse microscopy videos of fluorescent HaCaT cells (left) to cellular tracks (right). **B)** The Pathfinder program uses the positional information of cellular tracks to calculate speed, where  $dS$  represents change in position and  $dt$  represents change in time (top), migration persistence through the absolute angle of deflection (bottom), and the migration direction relative to a well-defined axis orientation in the field of view (right).  
doi:10.1371/journal.pone.0082444.g002

### Using the average absolute angle of deflection to measure cellular persistence

In order to provide a means for high throughput calculation of cellular migration persistence, we used a non-traditional, but direct, approach of calculating the angle of deflection for each cell at each time. **Fig. 2B**, bottom left, illustrates how the angle of deflection measures migration persistence. The diagram represents a single cell, whose position is measured at three successive time points (1, 2, and 3, respectively). As the cell travels from 1 to 2 it maps out a line representing the trajectory of the cell between these two times. Similarly, as the cell travels from 2 to 3, another line is formed. The angle of deflection is the angle between these two lines, where a clockwise turn has a positive value, and a counterclockwise turn has a negative value. Using this calculation, each cell at each time can be assigned an angle of deflection, such that the sampling of many cells at a single time point can provide an accurate measurement of how straight cells are migrating within the population. A decrease in the average absolute value of the angle of deflection for a population of cells ( $\langle |\theta_{\text{Deflection}}| \rangle$ ) reflects an increase in the migration persistence. We use the absolute value of the angle of deflection for describing the persistence of migration in large populations, rather than maintaining the sign of the angle of deflection, because cells do not display a bias in which direction they prefer to turn (**Fig. 3A**).

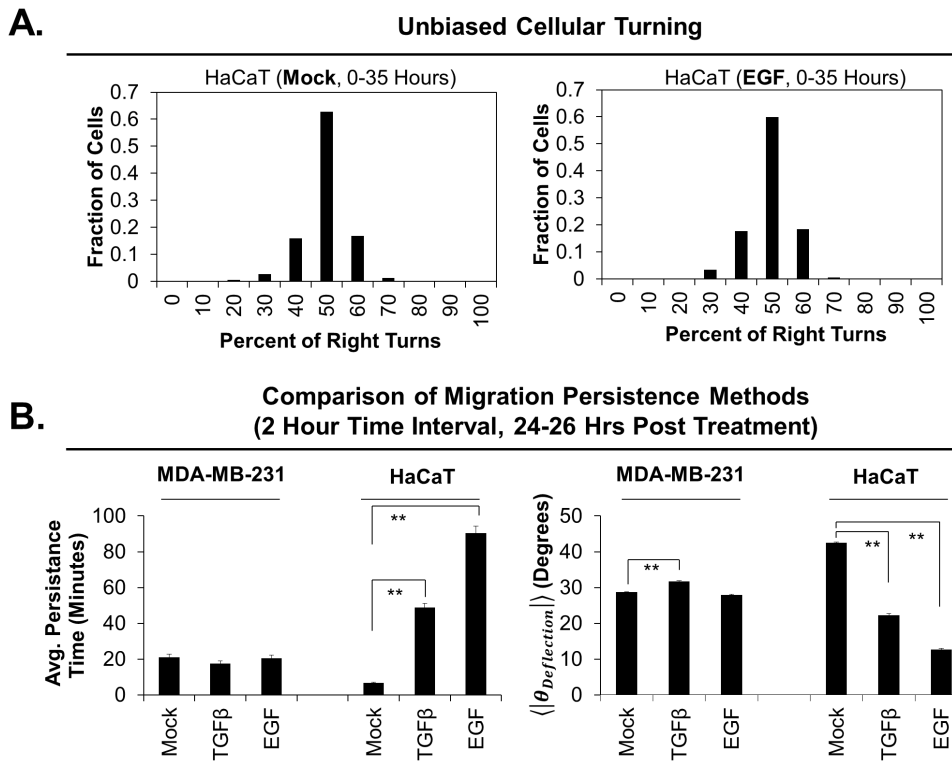


**Figure 3. Average absolute angle of deflection measurements accurately depict the migration persistence of cells. A)** Cells do not prefer to turn right or left in either the presence (right) or absence (left) of EGF stimulation. A binned histogram of percent of cells versus percent of right turns is normal and centered around 50 percent. **B)** A comparison of persistence time calculations and average absolute angle of deflection ( $\langle |\theta_{\text{deflection}}| \rangle$ ) methods for measuring migration persistence yields identical trends in both the presence and absence of either TGFβ or EGF for MDA-MB-231 cells and HaCaT cells. Double asterisks indicate a  $p$  value  $< 0.01$ . Each condition represents greater than 200 cells for persistence time measurements, and greater than 1000 cells for average absolute angle of deflection measurements. doi:10.1371/journal.pone.0082444.g003

**Comparing methods to measure migration persistence**

Although we measure migration persistence using the average absolute angle of deflection, the measurement of migration persistence is currently conducted in the cell migration field through the determination of persistence time, which is calculated using data fitting of time dependent mean squared displacement trends to Equation 1, where  $MSD$  is the mean squared displacement of the cell,  $n_d$  is the number of dimensions in which cells are migrating,  $S^2$  represents the squared speed of the cell,  $P$  represents the persistence time of a cell, and  $t$  is the time.

$$MSD = n_d S^2 P t \left[ 1 - \frac{P}{t} (1 - e^{-t/P}) \right] \tag{1}$$

Persistence time is used to measure migration persistence because local changes in mean squared displacements trends are likely to be associated with changes in the direction of cellular migration, provided that speed is taken into consideration. A key difference between our approach and the persistence time approach is that persistence time measurements focus on how long a cell maintains a direction, while the average absolute angle of deflection measurements focus on the degree to which cells in a population turn in each frame. Thus, persistence time measurements reflect behavior over a specified interval of time (usually 2–4 hours), while the average absolute angle of deflection measurements reflect the relatively instantaneous behavior of cells.

We compared our technique of measuring migration persistence to the method of measuring persistence time by examining the time-lapse microscopy videos of two cell lines, MDA-MB-231 and HaCaT, stably expressing fluorescent nuclear markers and treated with no ligand, TGFβ or EGF. When such videos of HaCaT cells (24–26 hours post ligand stimulation) are analyzed by the two methods, both techniques lead to the same conclusions; TGFβ and EGF stimulation cause increased migration persistence, where EGF has an impact of higher magnitude than that of TGFβ (Fig. 3B). Both methods also agree when the same analysis is applied to MDA-MB-231 cells, where only TGFβ has a low magnitude effect on migration persistence (Fig. 3B). The measured persistence time of approximately 30 minutes observed for EGF stimulated MDA-MB-231 cells is consistent with similar results from other studies [82]. Since these two techniques yield the same results under these experimental conditions, we conclude that both techniques accurately measure migration persistence in motile cells. However, there is one critical difference between our method for measuring migration persistence compared to the persistence time method. Measuring the average absolute angle of deflection can yield a measurement for migration direction for each frame, while persistence time calculations require enough frames to construct a MSD vs time plot to fit to Equation 1. Thus, the persistence time calculation, which is traditionally calculated from sampling over 2–4 hours, cannot accurately report when a cell turns and how much it turns, but instead reports its average tendency to turn. The value of having the ability to measure exactly when an to what degree a cell turns will prove useful for

future investigations into the mechanism by which cells are guided and will aid researchers in answering how exactly a cell determines where to extend its front end.

### Overlapping intervals suppresses noise in directional cellular behavior

The Pathfinder software is unique from other software in that it calculates angular information about individual cells. However, such angular information requires that the determination of a cell's position be relatively noise free. When we closely examine the tracks of individual cells, we find that tracks exhibit slight vibration on the short timescale (7 minutes), such that a cell that migrates relatively straight does not display a perfectly straight track. As a result, we use overlapping intervals for our calculations of angular information in order to suppress the effects of such vibration on angular calculations. The schematic diagram in **Fig. 4A** illustrates how overlapping intervals aid in the reduction of noise in the calculation of cellular speed, direction, and persistence. Presented is the path of a single hypothetical cell that travels from positions 1 to 6. When calculating the trajectory of the movement from position 1 to 2, the resulting vector does not accurately represent the underlying trajectory of the cell over time. However, as the calculation is repeated in the same manner for a change in position from 1 to increasing successive positions, the resulting vectors quickly converge on the underlying trajectory of the cell. Each interval represents the cellular behavior in a video that has a frame rate that is the (acquisition frame rate)  $\times$  (the interval size). For instance, if the interval size is 3 frames, then calculations are conducted on frames 1,4,7,10, and so forth. When successive intervals are combined, with a single frame shift from one interval to the next, the resulting data provides a time dependent parameter that has greatly suppressed noise.

**Fig. 4B and C** show the effect of increasing interval size on the time dependent average absolute angle of deflection trend and the average standard deviation of the absolute angle of deflection trend for HaCaT cells treated with TGF $\beta$ . With an interval size of 1 frame, both the average (**Fig. 4B**) and the error (**Fig. 4C**) of the angle deflection measurements are extremely noisy. With increasing interval size, such noise is suppressed, where an interval size of greater than 2 (corresponding to 14 minutes) does not yield significant additional suppression of noise. For all cellular experiments detailed in this investigation, an interval size of 3 frames was used. This method of overlapping intervals was applied to all measurements, with the exception of persistence time measurements.

### Measuring time dependent changes in migration persistence and speed

Upon mere qualitative assessment of cellular tracks, cellular behavior is difficult to deduce for large populations of cells. For example, when we examine MDA-MB-231 and HaCaT cell migration in response to either TGF $\beta$  or EGF by looking at the tracks of cells between 0 and 35 hours post ligand stimulation, MDA-MB-231 cells appear to not change behavior in response to ligand treatments and HaCaT cells appear to respond in the same manner upon TGF $\beta$  and EGF stimulation (**Fig. 5A and B**). However, MDA-MB-231 cells do in fact respond to ligand stimulations and HaCaT cells do in fact respond differently to TGF $\beta$  and EGF stimulation (**Movie S1 and S2**), which is elaborated upon below. Thus, only through rigorous quantitation can large populations be characterized for their cellular behavior.

Using our quantitative approach to measuring cellular migration, we were able to determine that either TGF $\beta$  or EGF causes

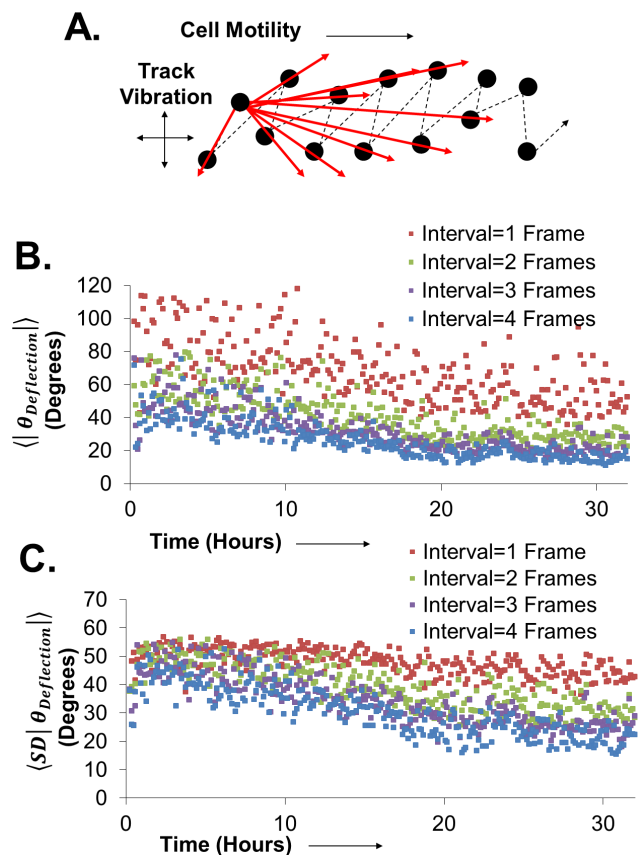


**Figure 4. Overlapping Intervals Suppress Angular Noise in Cellular Migration.** **A**) A schematic representation of a cellular track illustrates how increasing interval size results in the calculation of a cellular migration direction that is resistant to track vibration noise. **B**) The average absolute angle of deflection as a function of time for TGF $\beta$  treated HaCaT H2B mCherry cells for an interval size of one frame shows strong scattering of measurements. Upon increasing interval size, such scattering is suppressed. **C**) Such scattering can be also measured by measuring the standard deviation in the absolute angle of deflection, which can be suppressed in a similar manner by increasing interval size. Data represents greater than 1000 cells for each plot. doi:10.1371/journal.pone.0082444.g004

MDA-MB-231 cells to migrate faster, but has almost no effect on how persistently cells migrate. Only stimulation with TGF $\beta$  causes a statistically significant ( $p=0.003$ ), but extremely small in magnitude, decrease in migration persistence, as evident by a slight elevation in the average absolute angle of deflection of cells (**Fig. 5C, top left**). Both TGF $\beta$  and EGF treatments yield an increase in the average speed of these cells, where EGF response is early (approximately 1 hour) and TGF $\beta$  response is late (approximately 10 hours) (**Fig. 5C, bottom**). In contrast to MDA-MB-231 cells, both speed and migration persistence are activated by TGF $\beta$  and EGF treatment in HaCaT cells, where the effects of EGF appear early (approximately 1 hour) and the effects of TGF $\beta$  appear late (approximately 10 hours) (**Fig. 5D**). Through our rigorous quantitation method, we conclude that motility promoting ligand stimulations can differ greatly from each other in terms of both the effect on cellular migration parameters and the kinetics of activation, both of which can be determined using the Pathfinder program. Taken together, this data illustrates the importance of time resolution in measuring cell migration responses to environmental stimuli, as well as the importance of

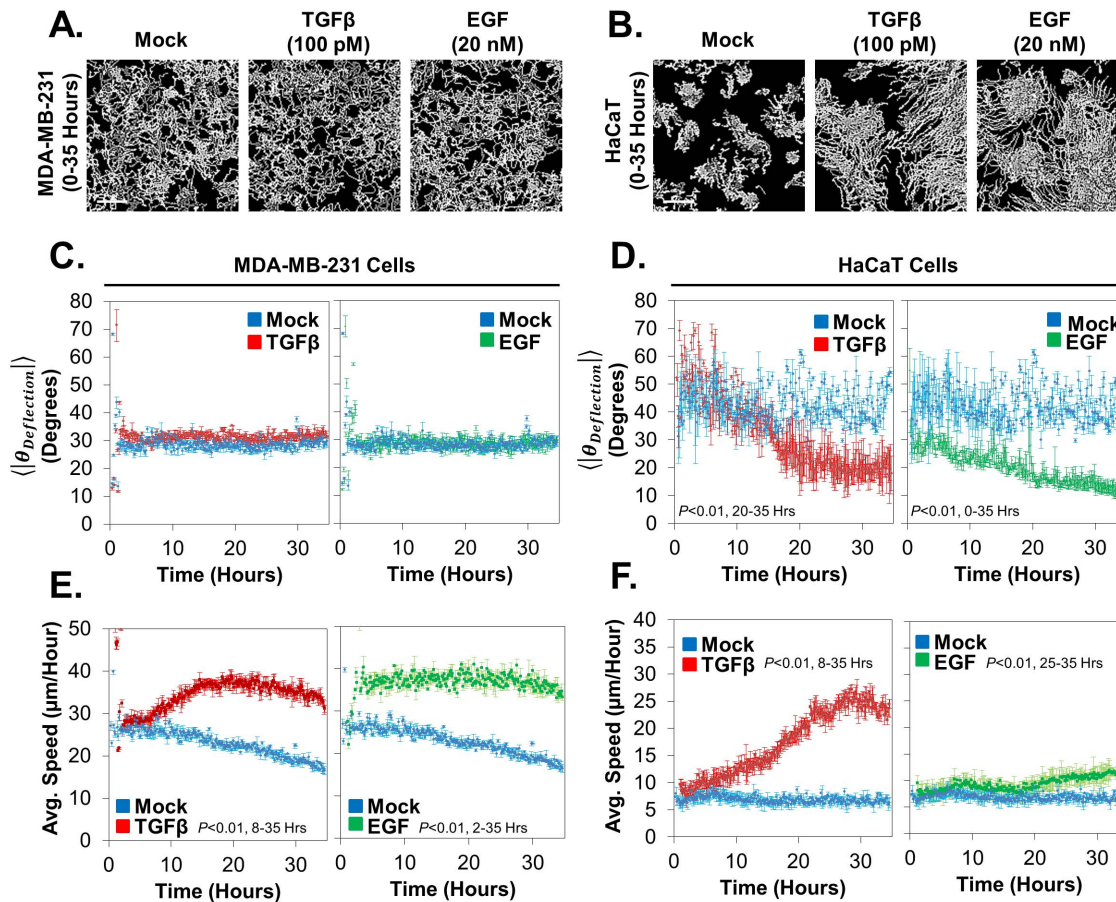


**Figure 5. Measuring individual cellular behavior with speed and migration persistence reveals cell type and ligand specific cellular migration behavior.** Cellular tracks of low density cells are displayed for treatments of either Mock, TGF $\beta$  or EGF for MDA-MB-231 cells (A) or HaCaT cells (B). Calibration bars represent 150  $\mu\text{m}$ . C) Neither TGF-Beta nor EGF stimulation affects migration persistence in MDA-MB-231 cells (top). In contrast, both treatments affect cellular speed, but with different induction kinetics (bottom). D) In HaCaT cells, both ligand treatments affect migration persistence and cellular speed (top and bottom, respectively). However, EGF stimulates migration persistence with earlier kinetics than that of TGF $\beta$  (top), and EGF is a poor stimulator of migration speed (bottom, right). Each condition represents greater than 1000 cells. doi:10.1371/journal.pone.0082444.g005

measuring both the speed and the persistence of cells in order to characterize the full behavior of cell migration.

### Quantifying collective migration with nearest neighbor analyses of angular measurements

The increasing interest in the collective behavior of cells in the cell migration field prompted us to integrate the capability of characterizing collective migration into the Pathfinder software. One already implemented method for measuring collective migration involves the calculation of the size of collectively migrating streams of cells [33]. Although this method is certainly a valid way to measure the ‘collectiveness’ of cells within a population of cells, it requires a predetermined threshold to identify whether or not neighboring cells are part of a migrating stream (a 10 degree difference in migration direction or less is required to group cells together as a collectively migrating stream). In contrast, we used Pathfinder and a matrix based calculation to provide an alternative method for measuring how similar pairs of neighboring cells are in the directions that they migrate. This method does not require any predetermined thresholds as mention above. For each cell, Pathfinder reports the angle of trajectory, or migration direction. For this parameter, each cell is assigned an angle that ranges from 0 to 359 degrees relative to a well-defined

set of axes in the field of view. Fig. 2B, right, illustrates the orientation of these axes in the field of view, and provides an example of a cell that is migrating in the direction of 45 degrees. In a similar manner to the case of angle of deflection, each cell gets such an assignment for each time, providing time resolution of cellular direction. In order to demonstrate how the angle of trajectory calculation can be used to characterize collective migration, we examined HaCaT and MDA-MB-231 cells in confluent monolayers in response to EGF stimulation. Manual inspection of the cellular tracks of these monolayers suggests that neighboring cells migrate in a similar direction in a ligand dependent manner in HaCaT cells (Fig. 6A, top). This behavior is not qualitatively observed for MDA-MB-231 cells (Fig. 6A, bottom). Since collective migration is defined as the ability of cells to adopt a common migration direction, we quantified the average standard deviation of the angle of trajectory, also referred to as the “paired random migration index” (PRMI  $\Theta_{\text{Trajectory}}$ ), amongst pairs of nearest neighboring cells at 22–26 hours post ligand stimulation. An increase in this quantity indicates that nearest neighboring cells are migrating in increasingly different directions, meaning collective migration is decreasing. We excluded pairs of neighbors in which one cell migrates with a direction of 0–90 degrees and another cell migrates in a direction of 270–360

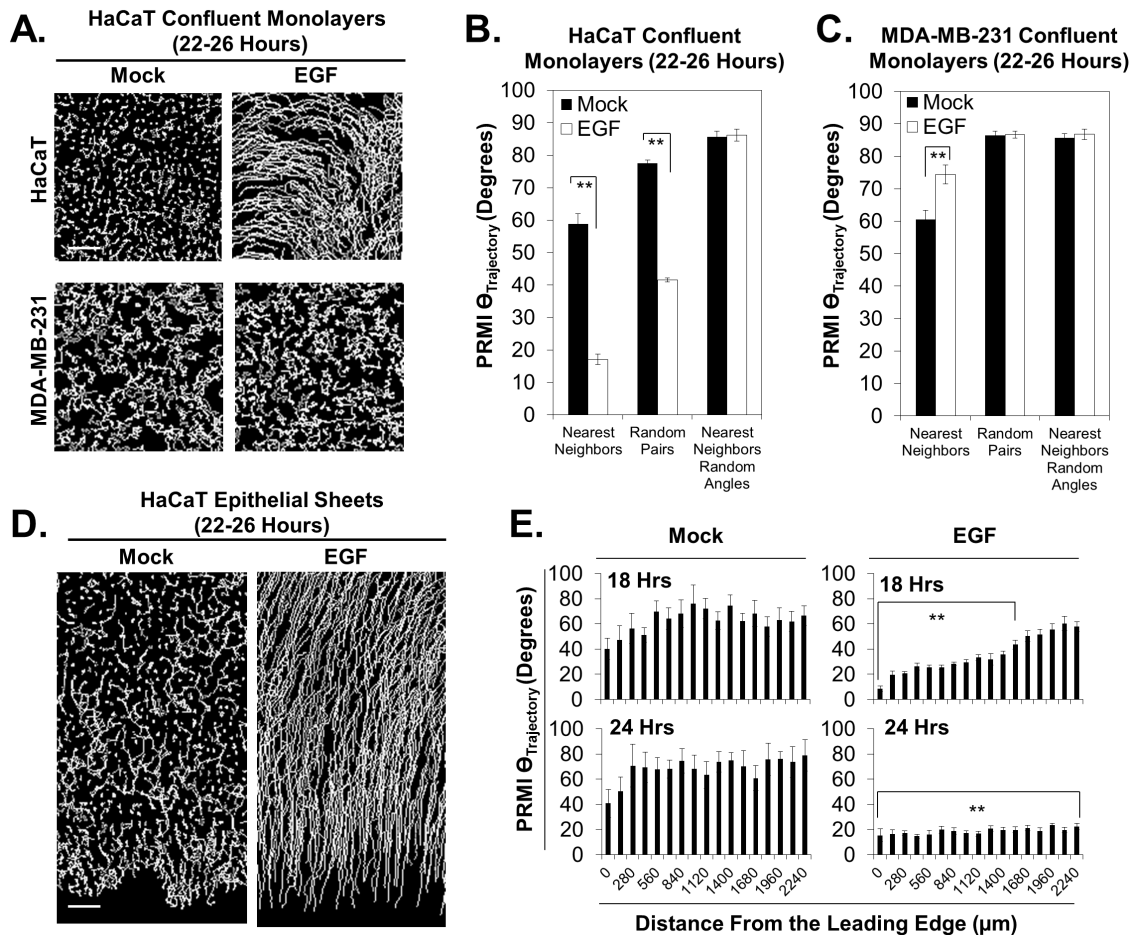


**Figure 6. Angular measurements can be used to quantify collective migration behavior.** **A)** Cellular tracks of confluent monolayers of HaCaT (top) and MDA-MB-231 cells (bottom) in the presence and absence of EGF stimulation. Calibration bar represents 150  $\mu\text{m}$ . **B)** Confluent monolayers of HaCaT cells in the presence and absence of EGF stimulation were quantified for their collective migration behavior by calculating the average standard deviation of the angle of trajectory (also called the paired random migration index (PRMI  $\Theta_{\text{Trajectory}}$ ) amongst nearest neighboring cells. Random pairing was used to determine whether the observed behavior was local or global amongst the population. **C)** The same quantification was conducted for MDA-MB-231 cells. **D)** Cellular tracks of epithelial sheets of HaCaT cells in the presence and absence of EGF stimulation. Calibration bar represents 150  $\mu\text{m}$ . **E)** Inspection of the spatial distribution of collective migration behavior reveals that EGF stimulation elicits collective migration that propagates away from the leading edge. Double asterisks indicate a  $p$  value < 0.01. doi:10.1371/journal.pone.0082444.g006

degrees, as these pairs would have a falsely high standard deviation due to the discontinuous transition between 360 degrees and 1 degree. In agreement with our qualitative observations of cellular tracks, nearest neighboring HaCaT cells display a lower PRMI  $\Theta_{\text{Trajectory}}$  in response to EGF stimulation (Fig. 6B). We compared nearest neighbor behavior to random pairing behavior in order to identify when shared behavior of cells is global versus local. If random pairing does not change the magnitude of the PRMI  $\Theta_{\text{Trajectory}}$ , then the shared behavior is entirely global. In contrast, when such magnitudes are affected by random pairing, the phenomenon is local. Upon random pairing of HaCaT cells, a similar trend is observed for the PRMI  $\Theta_{\text{Trajectory}}$ , but the magnitudes increase for both mock treatment and EGF treatment. Thus, EGF stimulation of HaCaT cells activates local collective migration, which diminishes with increasing distance between neighbors. As a control, we repeated our nearest neighbor calculations after substitution of random angles of trajectory (nearest neighbors random angles) in order to determine that the maximum value for the PRMI  $\Theta_{\text{Trajectory}}$  is approximately 85 degrees in both the presence and absence of EGF stimulation. This

maximum value is greater than that of the PRMI  $\Theta_{\text{Trajectory}}$  in the absence of ligand stimulation, revealing that HaCaT cells do display a small degree of collective migration, which we were not able to detect upon manual qualitative inspection of time-lapse videos. Using the same technique on MDA-MB-231 cells, we found that these cells display a statistically significant, but low magnitude, increase in the PRMI  $\Theta_{\text{Trajectory}}$  amongst nearest neighbors in response to EGF, suggesting that ligand stimulation of these cells causes neighboring cells to exhibit slight repulsion, and migrate more in opposing directions upon EGF stimulation (Fig. 6C). Random pairing of MDA-MB-231 cells led to an increase in the magnitude of the PRMI  $\Theta_{\text{Trajectory}}$ , revealing that the collective migration of these cells is entirely a local phenomenon. Substitution of random angles of trajectories into data sets revealed a similar maximum value for the PRMI  $\Theta_{\text{Trajectory}}$ , which was approximately 85 degrees. Whether or not the apparent collective migration behavior of neighboring MDA-MB-231 cells in the absence of ligand stimulation constitutes collective migration according to the accepted definition will require further investigation into the requirement of cellular



junctions in this process. However, it is worth noting that the neighboring cells do in fact have physical contact with each other (**Fig. S4**), albeit for short timescales (data not shown).

### Using nearest neighbor analyses of angular measurements to characterize collective migration in epithelial sheets

In order to determine the versatility of our method of collective migration quantification, we repeated our experiments on HaCaT cells using EGF stimulation, but under the condition in which cells were arranged into epithelial sheets (**Fig. 6D and Movie S3**). We asked whether or not ligand stimulation instantaneously affects all cells equally in an epithelial sheet, and found that the collective behavior response to EGF stimulation propagates away from the leading edge of an epithelial sheet overtime as indicated by propagation of decreasing PRMI  $\Theta_{\text{Trajectory}}$  away from the leading edge of an epithelial sheet (**Fig. 6E**). Thus, our technique of quantitatively characterizing collective migration has proven useful to determine the spatial collective migration properties throughout a population of cells.

## Discussion

### The pathfinder software provides novel useful tools for studying individual and collective cell migration

Our Pathfinder software is the first high throughput automated cell migration software to conduct measurements of instantaneous angular parameters for the quantification of cell migration behavior. Our parameter of the angle of deflection has proven useful for characterizing the migration persistence of cells in two dimensional fluorescence microscopy experiments. In addition to helping researchers investigate the molecular mechanisms behind migration persistence, this parameter can be used to identify the differential temporal responses of cells to distinct ligand stimulations, and can provide insight into the molecular mechanisms behind each ligand response. Furthermore, the available cell migration software has been entirely devoid of tools that can be used to readily quantify collective migration. As a result, investigations of collective migration have been more appropriately described as qualitative rather than quantitative. The Pathfinder software provides the first high throughput tool to quantitatively characterize collective cell migration using the angle of trajectory parameter, which can be used to determine the “Paired Random Migration Index” (PRMI  $\Theta_{\text{Trajectory}}$ ) amongst nearest neighbors. This tool is likely to propel the collective migration field forward, as it can provide a means for accurately measuring the degree to which cells are migrating collectively, with both spatial and temporal resolution. Our method of measuring collective migration was able to reveal hidden collective cellular behavior that cannot be easily detected qualitatively from cellular tracks, such as the local collective migration behavior amongst pairs of MDA-MB-231 cells, and the ability of EGF stimulation to suppress this behavior. In conclusion, our Pathfinder software provides novel techniques for characterizing cellular migration in a high throughput platform, which are likely to aid the cell migration field in its investigation of the molecular mechanisms behind individual and collective migration.

## Supporting Information

**Data S1 Pathfinder Program.** The Pathfinder program is an executable JAVA program that requires installation of JAVA Runtime Environment on a Windows operating system. (JAR)

**Data S2 A sample output from Pathfinder.** A sheet of HaCaT H2B-mCherry cells were analyzed for individual cell migration from a microscopy video between 22 and 25.5 hours post 100 nM EGF stimulation. Frames were acquired every 7 minutes. Analysis was conducted with a frame binning of 3 frames (21 minutes). (XLSX)

**Data S3 A MATLAB script to convert mean squared displacement (MSD) versus time data from a Pathfinder output into persistence time.** This MATLAB script requires user input of MSD and time data for each cell and converts this information into persistence time. (M)

**Figure S1 Parameter descriptions for the Pathfinder program GUI.** User input parameters are: Cell Outer Radius, Cell Minimum Radius (Cutoff), Percentage of Pixels with Nuclear Signal (Percentile), How Far an Average Cell is Tolerated to Migrate From Frame to Frame (Disp./Frame), How Many Frames to Bin for Calculations (Frame Binning), Minimum Tack Length (Min. Trajectory Length), Number of Parallel Threads (Threads), Folder Path for Folder with Videos (AVI Folder). (TIF)

**Figure S2 A description of output calculations from the Pathfinder program.** Each cell receives a cellular ID number (1), for each frame (2). In each frame a cell is assigned an X (3) and Y (4) coordinate, a displacement from the last frame in pixels (5), an angle of trajectory (6), an angle of deflection (7) and a mean squared displacement (8). Mean squared displacements can be used to calculate the persistence time for a cell. For the population of cells, Pathfinder reports the frame (9) dependent change in the average displacement (10), the average angle of trajectory (11), the percentage of cells turning greater than 90 degrees (12), and the average absolute angle of deflection (13). Additionally, Pathfinder reports a binned histogram of percent of cells versus the possible migration directions from 0 to 359 degrees (14 and 15). Lastly, the number of cellular tracks is reported (16). (TIF)

**Figure S3 Wild type MDA-MB-231 cells and MDA-MB-231 H2B-mCherry cells migrate with similar speeds in the presence and absence of EGF stimulation.** Brightfield microscopy videos of mock and EGF treated wild type (WT) MDA-MB-231 cells were manually measured for position over the course of a 10 frame interval (7 minutes/frame) after 24 hours ligand or mock stimulation and the average speed of cells was calculated with a frame binning of 3. The same analysis was done on parallel videos of MDA-MB-231 using pathfinder, which yielded similar results for WT and labeled cells in the speed of migration in the presence and absence of EGF. 50 cells were used for this comparison for each condition. (TIF)

**Figure S4 MDA-MB-231 cells maintain physical contact with their nearest neighboring cell.** Brightfield microscopy of EGF treated MDA-MB-231 cells reveals that nearest neighboring cells have physical contact with each other. (TIF)

**Movie S1 MDA-MB-231 cells at low density upon either mock, TGF $\beta$ , or EGF treatment.** MDA-MB-231 cells with an H2B-mCherry nuclear marker were observed by time-lapse microscopy using the mCherry fluorescence channel. Each frame represents 7 minutes. (AVI)

**Movie S2 HaCaT cells at low density upon either mock, TGF $\beta$ , or EGF treatment.** HaCaT cells with an H2B-mCherry nuclear marker were observed by time-lapse microscopy using the mCherry fluorescence channel. Each frame represents 7 minutes. (AVI)

**Movie S3 Epithelial sheets of HaCaT cells upon either mock or EGF treatment.** HaCaT cells with an H2B-mCherry nuclear marker were assembled into epithelial sheets and observed by time-lapse microscopy using the mCherry fluorescence channel. Each frame represents 7 minutes. (AVI)

## References

- Chambers AF, Groom AC, MacDonald IC (2002) Dissemination and growth of cancer cells in metastatic sites. *Nat Rev Cancer* 2: 563–572.
- Friedl P, Wolf K (2003) Tumour-cell invasion and migration: diversity and escape mechanisms. *Nat Rev Cancer* 3: 362–374.
- Keller R (2005) Cell migration during gastrulation. *Curr Opin Cell Biol* 17: 533–541.
- Locascio A, Nieto MA (2001) Cell movements during vertebrate development: integrated tissue behaviour versus individual cell migration. *Curr Opin Genet Dev* 11: 464–469.
- Montell DJ (2003) Border-cell migration: the race is on. *Nat Rev Mol Cell Biol* 4: 13–24.
- Wang W, Goswami S, Lapidus K, Wells AL, Wyckoff JB, et al. (2004) Identification and testing of a gene expression signature of invasive carcinoma cells within primary mammary tumors. *Cancer Res* 64: 8585–8594.
- Wang W, Goswami S, Sahai E, Wyckoff JB, Segall JE, et al. (2005) Tumor cells caught in the act of invading: their strategy for enhanced cell motility. *Trends Cell Biol* 15: 138–145.
- Abercrombie M (1979) Contact inhibition and malignancy. *Nature* 281: 259–262.
- Abercrombie M, Heaysman JE (1953) Observations on the social behaviour of cells in tissue culture. I. Speed of movement of chick heart fibroblasts in relation to their mutual contacts. *Exp Cell Res* 5: 111–131.
- Abercrombie M, Heaysman JE (1954) Invasiveness of sarcoma cells. *Nature* 174: 697–698.
- Horwitz R, Webb D (2003) Cell migration. *Curr Biol* 13: R756–759.
- Lauffenburger DA, Horwitz AF (1996) Cell migration: a physically integrated molecular process. *Cell* 84: 359–369.
- Van Haastert PJ, Devreotes PN (2004) Chemotaxis: signalling the way forward. *Nat Rev Mol Cell Biol* 5: 626–634.
- Rorth P (2009) Collective cell migration. *Annu Rev Cell Dev Biol* 25: 407–429.
- Rorth P (2007) Collective guidance of collective cell migration. *Trends Cell Biol* 17: 575–579.
- Bronner-Fraser M (1993) Neural crest cell migration in the developing embryo. *Trends Cell Biol* 3: 392–397.
- Lois C, Garcia-Verdugo JM, Alvarez-Buylla A (1996) Chain migration of neuronal precursors. *Science* 271: 978–981.
- Martin P (1997) Wound healing—aiming for perfect skin regeneration. *Science* 276: 75–81.
- Murase S, Horwitz AF (2004) Directions in cell migration along the rostral migratory stream: the pathway for migration in the brain. *Curr Top Dev Biol* 61: 135–152.
- Rorth P (2002) Initiating and guiding migration: lessons from border cells. *Trends Cell Biol* 12: 325–331.
- Xia Y, Karin M (2004) The control of cell motility and epithelial morphogenesis by Jun kinases. *Trends Cell Biol* 14: 94–101.
- Zhang L, Wang W, Hayashi Y, Jester JV, Birk DE, et al. (2003) A role for MEK kinase 1 in TGF- $\beta$ /activin-induced epithelium movement and embryonic eyelid closure. *Embo J* 22: 4443–4454.
- Abercrombie M, Heaysman JE (1954) Observations on the social behaviour of cells in tissue culture. II. Monolayering of fibroblasts. *Exp Cell Res* 6: 293–306.
- Ridley AJ, Schwartz MA, Burridge K, Firtel RA, Ginsberg MH, et al. (2003) Cell migration: integrating signals from front to back. *Science* 302: 1704–1709.
- Fischer RS, Gardel M, Ma X, Adelstein RS, Waterman CM (2009) Local cortical tension by myosin II guides 3D endothelial cell branching. *Curr Biol* 19: 260–265.
- Friedl P, Noble PB, Walton PA, Laird DW, Chauvin PJ, et al. (1995) Migration of coordinated cell clusters in mesenchymal and epithelial cancer explants in vitro. *Cancer Res* 55: 4557–4560.
- Ghabrial A, Luschnig S, Metzstein MM, Krasnow MA (2003) Branching morphogenesis of the *Drosophila* tracheal system. *Annu Rev Cell Dev Biol* 19: 623–647.
- Khalil AA, Friedl P (2010) Determinants of leader cells in collective cell migration. *Integr Biol (Camb)* 2: 568–574.
- Prasad M, Montell DJ (2007) Cellular and molecular mechanisms of border cell migration analyzed using time-lapse live-cell imaging. *Dev Cell* 12: 997–1005.
- Theveneau E, Marchant L, Kuriyama S, Gull M, Moepps B, et al. (2010) Collective chemotaxis requires contact-dependent cell polarity. *Dev Cell* 19: 39–53.
- Vitorino P, Hammer M, Kim J, Meyer T (2011) A steering model of endothelial sheet migration recapitulates monolayer integrity and directed collective migration. *Mol Cell Biol* 31: 342–350.
- Vitorino P, Meyer T (2008) Modular control of endothelial sheet migration. *Genes Dev* 22: 3268–3281.
- Slater B, Londono C, McGuigan AP (2013) An algorithm to quantify correlated collective cell migration behavior. *Biotechniques* 54: 87–92.
- Chen Y, Dodd SJ, Tangrea MA, Emmert-Buck MR, Koretsky AP (2013) Measuring collective cell movement and extracellular matrix interactions using magnetic resonance imaging. *Sci Rep* 3: 1879.
- Rosello C, Ballet P, Planus E, Tracqui P (2004) Model driven quantification of individual and collective cell migration. *Acta Biotheor* 52: 343–363.
- dos Remedios CG, Chhabra D, Kekic M, Dedova IV, Tsubakihara M, et al. (2003) Actin binding proteins: regulation of cytoskeletal microfilaments. *Physiol Rev* 83: 433–473.
- Cory GO, Ridley AJ (2002) Cell motility: braking WAVES. *Nature* 418: 732–733.
- Etienne-Manneville S, Hall A (2002) Rho GTPases in cell biology. *Nature* 420: 629–635.
- Itoh RE, Kurokawa K, Ohba Y, Yoshizaki H, Mochizuki N, et al. (2002) Activation of rac and cdc42 video imaged by fluorescent resonance energy transfer-based single-molecule probes in the membrane of living cells. *Mol Cell Biol* 22: 6582–6591.
- Mogilner A, Oster G (1996) Cell motility driven by actin polymerization. *Biophys J* 71: 3030–3045.
- Ridley AJ, Hall A (1992) The small GTP-binding protein rho regulates the assembly of focal adhesions and actin stress fibers in response to growth factors. *Cell* 70: 389–399.
- Worthylake RA, Burridge K (2003) RhoA and ROCK promote migration by limiting membrane protrusions. *J Biol Chem* 278: 13578–13584.
- Pollard TD, Borisy GG (2003) Cellular motility driven by assembly and disassembly of actin filaments. *Cell* 112: 453–465.
- Welch MD, Mullins RD (2002) Cellular control of actin nucleation. *Annu Rev Cell Dev Biol* 18: 247–288.
- Rafelski SM, Theriot JA (2004) Crawling toward a unified model of cell motility: spatial and temporal regulation of actin dynamics. *Annu Rev Biochem* 73: 209–239.
- Condeelis JS, Wyckoff JB, Bailly M, Pestell R, Lawrence D, et al. (2001) Lamellipodia in invasion. *Semin Cancer Biol* 11: 119–128.
- Hussain NK, Jenna S, Glogauer M, Quinn CC, Wasiak S, et al. (2001) Endocytic protein intersectin-1 regulates actin assembly via Cdc42 and N-WASP. *Nat Cell Biol* 3: 927–932.
- Soderling SH, Binns KL, Wayman GA, Davee SM, Ong SH, et al. (2002) The WRP component of the WAVE-1 complex attenuates Rac-mediated signalling. *Nat Cell Biol* 4: 970–975.
- Nobes CD, Hall A (1995) Rho, rac, and cdc42 GTPases regulate the assembly of multimolecular focal complexes associated with actin stress fibers, lamellipodia, and filopodia. *Cell* 81: 53–62.
- Kurokawa K, Itoh RE, Yoshizaki H, Nakamura YO, Matsuda M (2004) Coactivation of Rac1 and Cdc42 at lamellipodia and membrane ruffles induced by epidermal growth factor. *Mol Biol Cell* 15: 1003–1010.
- Moissoglu K, Schwartz MA (2006) Integrin signalling in directed cell migration. *Biol Cell* 98: 547–555.
- Galbraith CG, Yamada KM, Galbraith JA (2007) Polymerizing actin fibers position integrins primed to probe for adhesion sites. *Science* 315: 992–995.

## Acknowledgments

We would like to thank Aaron Meyer and Dr. Doug Lauffenburger for making available a MATLAB program capable of calculating migration persistence according to equation 1. We also want to thank William St. Charles, Drew Goldberg, Adam Huckaby for the initial development of the PathFinder project as a part of the required assignment for Algorithms for Molecular Biology Course taught by Professor Debra Goldberg at the University of Colorado-Boulder in 2011. We thank Dr. Golberg for her inputs and support for this project.

## Author Contributions

Conceived and designed the experiments: DAC XL. Performed the experiments: DAC. Analyzed the data: DAC JJ. Contributed reagents/materials/analysis tools: XL. Wrote the paper: DAC XL.

53. Burridge K, Chrzanowska-Wodnicka M, Zhong C (1997) Focal adhesion assembly. *Trends Cell Biol* 7: 342–347.
54. Webb DJ, Parsons JT, Horwitz AF (2002) Adhesion assembly, disassembly and turnover in migrating cells – over and over and over again. *Nat Cell Biol* 4: E97–100.
55. Burridge K, Chrzanowska-Wodnicka M (1996) Focal adhesions, contractility, and signaling. *Annu Rev Cell Dev Biol* 12: 463–518.
56. Ren XD, Kiosses WB, Sieg DJ, Otey CA, Schlaepfer DD, et al. (2000) Focal adhesion kinase suppresses Rho activity to promote focal adhesion turnover. *J Cell Sci* 113 (Pt 20): 3673–3678.
57. Webb DJ, Donais K, Whitmore LA, Thomas SM, Turner CE, et al. (2004) FAK-Src signalling through paxillin, ERK and MLCK regulates adhesion disassembly. *Nat Cell Biol* 6: 154–161.
58. Burridge K, Turner CE, Romer LH (1992) Tyrosine phosphorylation of paxillin and pp125FAK accompanies cell adhesion to extracellular matrix: a role in cytoskeletal assembly. *J Cell Biol* 119: 893–903.
59. Cuevas BD, Abell AN, Witowsky JA, Yujiri T, Johnson NL, et al. (2003) MEKK1 regulates calpain-dependent proteolysis of focal adhesion proteins for rear-end detachment of migrating fibroblasts. *Embo J* 22: 3346–3355.
60. Lee J, Ishihara A, Oxford G, Johnson B, Jacobson K (1999) Regulation of cell movement is mediated by stretch-activated calcium channels. *Nature* 400: 382–386.
61. Ware MF, Wells A, Lauffenburger DA (1998) Epidermal growth factor alters fibroblast migration speed and directional persistence reciprocally and in a matrix-dependent manner. *J Cell Sci* 111 (Pt 16): 2423–2432.
62. Xie H, Pallero MA, Gupta K, Chang P, Ware MF, et al. (1998) EGF receptor regulation of cell motility: EGF induces disassembly of focal adhesions independently of the motility-associated PLCgamma signaling pathway. *J Cell Sci* 111 (Pt 5): 615–624.
63. Gail MH, Boone CW (1970) The locomotion of mouse fibroblasts in tissue culture. *Biophys J* 10: 980–993.
64. Hall A (1994) Small GTP-binding proteins and the regulation of the actin cytoskeleton. *Annu Rev Cell Biol* 10: 31–54.
65. Houk AR, Jilkine A, Mejean CO, Boltyanskiy R, Dufresne ER, et al. (2012) Membrane tension maintains cell polarity by confining signals to the leading edge during neutrophil migration. *Cell* 148: 175–188.
66. Mitra SK, Hanson DA, Schlaepfer DD (2005) Focal adhesion kinase: in command and control of cell motility. *Nat Rev Mol Cell Biol* 6: 56–68.
67. Small JV, Kaverina I (2003) Microtubules meet substrate adhesions to arrange cell polarity. *Curr Opin Cell Biol* 15: 40–47.
68. Srinivasan S, Wang F, Glavas S, Ott A, Hofmann F, et al. (2003) Rac and Cdc42 play distinct roles in regulating PI(3,4,5)P3 and polarity during neutrophil chemotaxis. *J Cell Biol* 160: 375–385.
69. Weber GF, Bjerke MA, DeSimone DW (2012) A mechanoresponsive cadherin-keratin complex directs polarized protrusive behavior and collective cell migration. *Dev Cell* 22: 104–115.
70. Zamir E, Geiger B (2001) Molecular complexity and dynamics of cell-matrix adhesions. *J Cell Sci* 114: 3583–3590.
71. Bray K, Brakebusch C, Vargo-Gogola T (2011) The Rho GTPase Cdc42 is required for primary mammary epithelial cell morphogenesis in vitro. *Small GTPases* 2: 247–258.
72. Osmani N, Peglion F, Chavrier P, Etienne-Manneville S (2010) Cdc42 localization and cell polarity depend on membrane traffic. *J Cell Biol* 191: 1261–1269.
73. Sieg DJ, Hauck CR, Ilic D, Klingbeil CK, Schaefer E, et al. (2000) FAK integrates growth-factor and integrin signals to promote cell migration. *Nat Cell Biol* 2: 249–256.
74. Sieg DJ, Hauck CR, Schlaepfer DD (1999) Required role of focal adhesion kinase (FAK) for integrin-stimulated cell migration. *J Cell Sci* 112 (Pt 16): 2677–2691.
75. Cukierman E, Pankov R, Stevens DR, Yamada KM (2001) Taking cell-matrix adhesions to the third dimension. *Science* 294: 1708–1712.
76. Fraley SI, Feng Y, Krishnamurthy R, Kim DH, Celedon A, et al. (2010) A distinctive role for focal adhesion proteins in three-dimensional cell motility. *Nat Cell Biol* 12: 598–604.
77. Tang H, Li A, Bi J, Veltman DM, Zech T, et al. (2013) Loss of Scar/WAVE complex promotes N-WASP- and FAK-dependent invasion. *Curr Biol* 23: 107–117.
78. Kostic A, Lynch CD, Sheetz MP (2009) Differential matrix rigidity response in breast cancer cell lines correlates with the tissue tropism. *PLoS One* 4: e6361.
79. Boldajipour B, Mahabaleswar H, Kardash E, Reichman-Fried M, Blaser H, et al. (2008) Control of chemokine-guided cell migration by ligand sequestration. *Cell* 132: 463–473.
80. Tang Q, Adams JY, Tooley AJ, Bi M, Fife BT, et al. (2006) Visualizing regulatory T cell control of autoimmune responses in nonobese diabetic mice. *Nat Immunol* 7: 83–92.
81. Wolf K, Wu YI, Liu Y, Geiger J, Tam E, et al. (2007) Multi-step pericellular proteolysis controls the transition from individual to collective cancer cell invasion. *Nat Cell Biol* 9: 893–904.
82. Harms BD, Bassi GM, Horwitz AR, Lauffenburger DA (2005) Directional persistence of EGF-induced cell migration is associated with stabilization of lamellipodial protrusions. *Biophys J* 88: 1479–1488.
83. Huth J, Buchholz M, Kraus JM, Molhave K, Gradinaru C (2011) Time-LapseAnalyzer: multi-target analysis for live-cell imaging and time-lapse microscopy. *Comput Methods Programs Biomed* 104: 227–234.
84. Huth J, Buchholz M, Kraus JM, Schmucker M, von Wichert G (2010) Significantly improved precision of cell migration analysis in time-lapse video microscopy through use of a fully automated tracking system. *BMC Cell Biol* 11: 24.
85. Joslin EJ, Opreko LK, Wells A, Wiley HS, Lauffenburger DA (2007) EGF-receptor-mediated mammary epithelial cell migration is driven by sustained ERK signaling from autocrine stimulation. *J Cell Sci* 120: 3688–3699.
86. Platek A, Mettlen M, Camby I, Kiss R, Amyere M, et al. (2004) v-Src accelerates spontaneous motility via phosphoinositide 3-kinase, phospholipase C and phospholipase D, but abrogates chemotaxis in Rat-1 and MDCK cells. *J Cell Sci* 117: 4849–4861.
87. Sawyer C, Sturge J, Bennett DC, O'Hare MJ, Allen WE, et al. (2003) Regulation of breast cancer cell chemotaxis by the phosphoinositide 3-kinase p110delta. *Cancer Res* 63: 1667–1675.
88. Sturge J, Hamelin J, Jones GE (2002) N-WASP activation by a beta1-integrin-dependent mechanism supports PI3K-independent chemotaxis stimulated by urokinase-type plasminogen activator. *J Cell Sci* 115: 699–711.
89. Sbalzarini IF, Koumoutsakos P (2005) Feature point tracking and trajectory analysis for video imaging in cell biology. *J Struct Biol* 151: 182–195.